OPEN ACCESS

KING'S College LONDON

King's Research Portal

DOI:
10.1073/pnas.1208916109

Document Version
Publisher's PDF, also known as Version of record

Link to publication record in King's Research Portal

Citation for published version (APA):
Boonrungsiman, S., Gentleman, E., Carzaniga, R., Evans, N. D., McComb, D. W., Porter, A. E., & Stevens, M. M. (2012). The role of intracellular calcium phosphate in osteoblast-mediated bone apatite formation. *Proceedings of the National Academy of Sciences of the United States of America*, *109*(35), 14170-14175. https://doi.org/10.1073/pnas.1208916109

Citing this paper
Please note that where the full-text provided on King's Research Portal is the Author Accepted Manuscript or Post-Print version this may differ from the final Published version. If citing, it is advised that you check and use the publisher's definitive version for pagination, volume/issue, and date of publication details. And where the final published version is provided on the Research Portal, if citing you are again advised to check the publisher's website for any subsequent corrections.

General rights
Copyright and moral rights for the publications made accessible in the Research Portal are retained by the authors and/or other copyright owners and it is a condition of accessing publications that users recognize and abide by the legal requirements associated with these rights.

•Users may download and print one copy of any publication from the Research Portal for the purpose of private study or research.
•You may not further distribute the material or use it for any profit-making activity or commercial gain
•You may freely distribute the URL identifying the publication in the Research Portal

Take down policy
If you believe that this document breaches copyright please contact librarypure@kcl.ac.uk providing details, and we will remove access to the work immediately and investigate your claim.

Download date: 04. May. 2023

The role of intracellular calcium phosphate in osteoblast-mediated bone apatite formation

Suwimon Boonrungsiman[a], Eileen Gentleman[a,b,c], Raffaella Carzaniga[d], Nicholas D. Evans[a,b,1], David W. McComb[a,e], Alexandra E. Porter[a,2], and Molly M. Stevens[a,b,f,2]

Departments of [a]Materials and [f]Bioengineering, [b]Institute of Biomedical Engineering, and [d]Electron Microscopy Centre, Division of Molecular Biosciences, Imperial College London, London SW7 2AZ, United Kingdom; [c]Craniofacial Development and Stem Cell Biology, King's College London, London SE1 9RT, United Kingdom; and [e]Department of Materials Science and Engineering, The Ohio State University, Columbus, OH 43210

Edited* by Robert Langer, Massachusetts Institute of Technology, Cambridge, MA, and approved July 16, 2012 (received for review June 5, 2012)

Mineralization is a ubiquitous process in the animal kingdom and is fundamental to human development and health. Dysfunctional or aberrant mineralization leads to a variety of medical problems, and so an understanding of these processes is essential to their mitigation. Osteoblasts create the nano-composite structure of bone by secreting a collagenous extracellular matrix (ECM) on which apatite crystals subsequently form. However, despite their requisite function in building bone and decades of observations describing intracellular calcium phosphate, the precise role osteoblasts play in mediating bone apatite formation remains largely unknown. To better understand the relationship between intracellular and extracellular mineralization, we combined a sample-preparation method that simultaneously preserved mineral, ions, and ECM with nano-analytical electron microscopy techniques to examine osteoblasts in an in vitro model of bone formation. We identified calcium phosphate both within osteoblast mitochondrial granules and intracellular vesicles that transported material to the ECM. Moreover, we observed calcium-containing vesicles conjoining mitochondria, which also contained calcium, suggesting a storage and transport mechanism. Our observations further highlight the important relationship between intracellular calcium phosphate in osteoblasts and their role in mineralizing the ECM. These observations may have important implications in deciphering both how normal bone forms and in understanding pathological mineralization.

biomineralization | crystallinity | mineral transport | electron energy-loss spectroscopy

The structure of bone stems from a tightly controlled process whereby collagen fibrils secreted by osteoblasts are progressively mineralized by poorly crystalline carbonated apatite. The process that precedes mineral's eventual propagation on the extracellular matrix (ECM), however, remains largely unexplained and is highly controversial. Investigators have proposed various mechanisms to explain early bone mineral formation including: (*i*) a cell-independent process, whereby charged noncollagenous proteins associating with the gap zones in collagen mediate mineral nucleation from ions in solution (1); (*ii*) a cell-controlled mechanism by which vesicles that bud from the plasma membrane accumulate ions extracellularly, mediate calcium phosphate precipitation, and subsequently rupture dispersing their contents on the ECM (2); and (*iii*) an alternative route by which amorphous mineral precursors are transiently produced and deposited within collagen fibrils, where they transform into more crystalline apatite platelets (3).

After decades of support for the former ion-based nucleation models (4), evidence has recently emerged supporting a role for the latter proposal, implicating amorphous mineral precursors in bone mineralization. For example, recent in vivo studies in mineralizing zebrafish fin rays (3, 5), and in vitro models of apatite formation on collagen fibrils (6) and nucleating surfaces (7) suggest that bone mineral creation proceeds via the transient formation of amorphous calcium phosphate. This process is biologically ubiquitous, analogous to that used by invertebrates, including mollusks and sea urchins, when creating their shells (8). The origin of the proposed amorphous calcium phosphate, however, is still unclear, and it also remains uncertain if the process is mediated by resident cells and, if so, whether the material forms intra- or extracellularly. Calcium phosphate deposits are known to reside intracellularly in mineralizing cells, notably as granules in mitochondria (9–11); however, their role in the mineralization process has never been definitively established. Mahamid et al. have also recently reported that calcium phosphate-containing vesicles are present in developing mouse bone cells (12); however, direct observations linking such intracellular deposits with the extracellular mineralization process have, until now, been lacking.

Results and Discussion

To investigate the relationship between intracellular calcium phosphate accumulations and extracellular bone apatite formation, we cultured mouse calvarial osteoblasts and marrow stromal cells (MSC) in osteogenic medium according to standard in vitro methods for bone-like nodule formation (13). We have previously demonstrated by multivariate analyses of micro-Raman spectra that such live, unprocessed nodules possess important characteristics of native bone, including the presence of a complex combination of mineral and matrix environments (14). Mineralized nodules formed from osteoblasts, when prepared by chemical fixation and analyzed by bright-field transmission electron microscopy (TEM), contained morphologically normal cells surrounded by a fibrous ECM (Fig. 1*A*) with banding typical of native mammalian collagen (Fig. 1*A*, *Inset*). Vesicles enclosing electron dense material composed of calcium and phosphorus as determined by energy dispersive X-ray spectroscopy (EDX) were evident within cells (Fig. 1*B*, and Figs. S1 and S2), within membrane invaginations (Fig. 1*C*) and immediately outside plasma membranes (Fig. 1*D*). Although the presence of plate- or needle-like ribbons within the vesicles indicates that the calcium phosphate has partially crystallized, it is well known that chemical fixation can cause the artifactual crystallization of calcium phosphate: amorphous calcium phosphate is thermodynamically unstable in aqueous environments and quickly converts to a more stable, crystalline phase of hydroxyapatite (15). Because of this possibility, we also chose to examine mineral crystallinity using

Author contributions: S.B., E.G., N.D.E., A.E.P., and M.M.S. designed research; S.B., E.G., and N.D.E. performed research; R.C. and D.W.M. contributed new reagents/analytic tools; S.B., E.G., N.D.E., and A.E.P. analyzed data; N.D.E., A.E.P., and M.M.S. revised the paper; and E.G. wrote the paper.

The authors declare no conflict of interest.

*This Direct Submission article had a prearranged editor.

[1]Present address: Human Development and Health Unit, Bioengineering Sciences Group, University of Southampton, Southampton SO16 6YD, UK.

[2]To whom correspondence may be addressed. E-mail: a.porter@imperial.ac.uk or m.stevens@imperial.ac.uk.

This article contains supporting information online at www.pnas.org/lookup/suppl/doi:10.1073/pnas.1208916109/-/DCSupplemental.

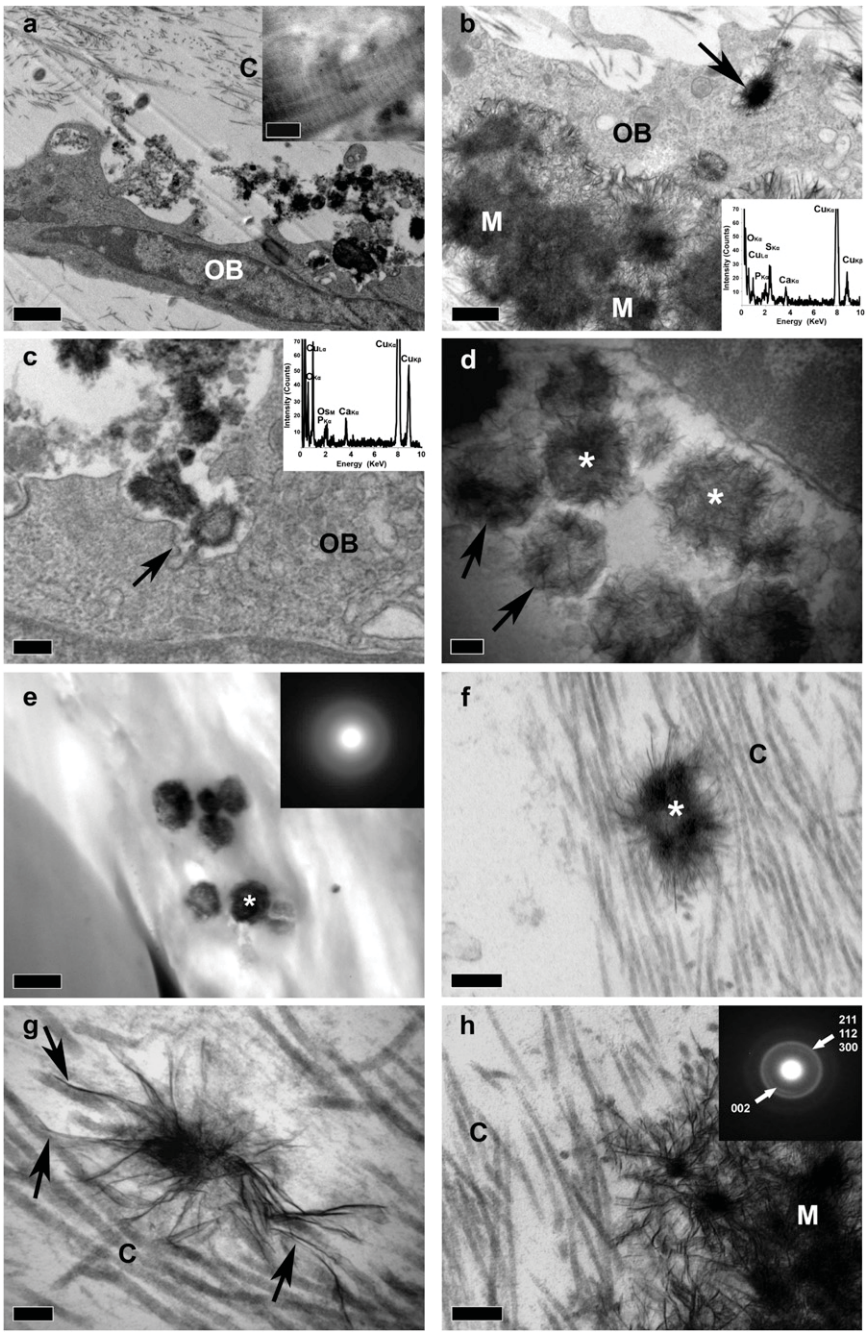

Fig. 1. Bright-field TEM images outlining intracellularly produced, vesicle-mediated mineralization in mouse osteoblast cultures. (*A*) Osteoblast (OB) embedded within a mineralized nodule. Fibrous extracellular matrix (C) with banding typical of mammalian collagen (*Inset*; Scale bar, 200 nm) surrounds the cell. Electron dense particles of bone-like mineral are evident in the extracellular space. Sample was prepared via the chemical fixation protocol. (Scale bar, 1 μm.) (*B*) A vesicle (arrow) containing electron dense material inside an osteoblast abutting a heavily mineralized (M) area of a nodule. EDX analysis of the material within the vesicle demonstrates the presence of calcium and phosphorus (*Inset*). Sample was prepared via the chemical fixation protocol. (Scale bar, 0.5 μm.) (*C*) Electron-dense vesicles within a membrane invagination (arrow) of an osteoblast. EDX analysis of the vesicle demonstrates the presence of calcium and phosphorus (*Inset*). Sample was prepared via the chemical fixation protocol. (Scale bar, 0.2 μm.) (*D*) Calcium phosphate-containing vesicles in the extracellular space surrounding an osteoblast. Sample was prepared via the chemical fixation protocol. (Scale bar, 0.2 μm.) (*E*) Confined calcium phosphate aggregates (membranes are not distinguishable in anhydrously prepared specimens) in a mineralized nodule prepared via the anhydrous fixation protocol. Selected area electron diffraction of an aggregate (*) lacks a textured crystalline diffraction pattern, suggesting the amorphous nature of the material (*Inset*). (Scale bar, 0.5 μm.) (*F*) A dense calcium phosphate aggregate (*) associated with collagen fibrils in the extracellular space. Sample was prepared via the chemical fixation protocol. (Scale bar, 0.2 μm.) (*G*) Mineral (arrows) emanating from the dense focus of a mineral aggregate associated with the collagenous extracellular matrix (C). Sample was prepared via the chemical fixation protocol. (Scale bar, 0.2 μm.) (*H*) Extensive mineralization (M) on collagen fibrils (C) in the extracellular space of a mineralized nodule formed from osteoblasts. Sample was prepared via the chemical fixation protocol. Selected area electron diffraction of a similarly mineralized area processed via the anhydrous fixation method displayed a crystalline diffraction pattern which corresponded to the 002, 112, 211, and 300 planes of a crystalline hydroxyapatite standard (*Inset*). (Scale bar, 0.2 μm.)

anhydrously prepared samples. Analysis of anhydrously prepared nodules by selected area electron diffraction (SAED, ~200-nm spot size) indicated that confined packets of calcium phosphate did not exhibit the textured crystalline diffraction pattern associated with developed mineral (15) (Fig. 1*E*). This finding indicates that calcium phosphate contained within the vesicles is either completely amorphous or a small amount of crystallinity (on the order of several unit cells) is present, which would give rise to the broadened rings in the SAED we observed here. This latter notion is supported by higher resolution phase-contrast images of the material within vesicles, which shows fine regions with crystalline order of the order of a few nanometers (Fig. S3) and could reflect the transient formation of intermediate mineral phases. In direct contrast to this finding, we observed mineral crystals associated with the collagenous ECM (Fig. 1*F* and Fig. S4) and emanating from dense foci (Fig. 1 *G* and *H*). SAED of similar areas in anhydrously prepared samples displayed a clear, textured crystalline diffraction pattern (Fig. 1*H*, *Inset*). Taken together, this sequence of images strongly supports the notion that calcium phosphate, devoid of any long-range order, is transported from inside the cell to the extracellular environment.

Calcium phosphate-containing vesicles, often referred to as "matrix vesicles," have been implicated in the mineralization of cartilage, bone, and dentin (16–18). However, previous observations have detected such vesicles extracellularly as they bud from the plasma membrane and subsequently accumulate mineral (17). Our observation here that calcium and phosphorus-containing vesicles also exist intracellularly is in keeping with recent observations of intracellular, vesicle-enclosed calcium phosphate in developing mouse bone (12), and suggests that an intracellular process may play a role in bone apatite formation. It is difficult to observe any such intracellular process, however, as conventional EM preparation techniques, such as glutaraldehyde fixation, preserve only cell structures and the proteinaceous ECM, but

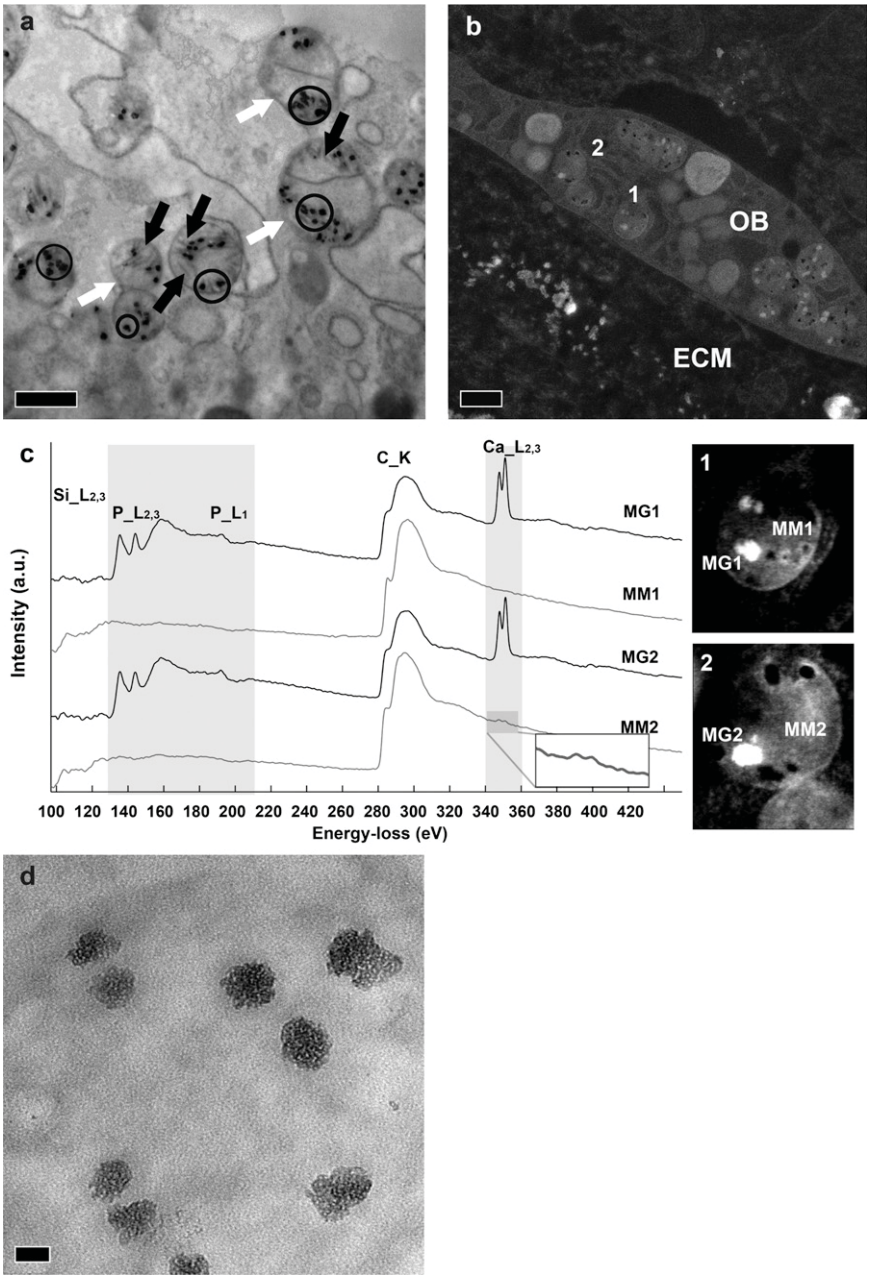

Fig. 2. Analytical electron microscopy evidence of calcium- and phosphorus-containing mineral aggregates in osteoblast mitochondria. (*A*) Bright-field TEM image demonstrating electron dense granules (circled) within the mitochondria (white arrows) of an osteoblast within a mineralized nodule. Mitochondria are readily identified by their characteristic cristae (black arrows). Sample was prepared by HPF-FS. (Scale bar, 0.5 μm.) (*B*) HAADF scanning TEM image of an osteoblast within a mineralized nodule. Dense granule-containing mitochondria are evident throughout the cell. Mitochondria indicated as 1 and 2 are analyzed further in *C*. Sample was prepared by HPF-FS protocol. (Scale bar, 0.5 μm.) (*C*) EELS of specified areas within mitochondria of a mineralizing osteoblast. Images 1 and 2 indicate the positions at which spectra were collected and highlight the presence of calcium and phosphorus in dense granules (MG1 and MG2) with characteristic phosphorus $L_{2,3}$ and calcium $L_{2,3}$ edges at 132 and 346 eV, respectively. The phosphorus $L_{2,3}$ edge contains characteristic double peaks (separated by 8.8 eV) followed by a more intense broad peak, which correlates with the phosphorus $L_{2,3}$ edge of analogous X-ray adsorption near edge structure (XANES) spectra acquired for phosphate compounds (22). Spectra collected within the less electron-dense areas of the mitochondrial matrix lack characteristic phosphorus edges (MM1 and MM2); however, MM2 produced an edge at 346 eV, indicative of calcium. All spectra contain distinctive carbon K edges at 285 eV. (*D*) Bright-field TEM image of mitochondrial granules within an osteoblast. Note that the granules consist of globular accumulations of mineral with a disordered morphology. Sample was prepared by high pressure freezing and freeze substitution protocol. (Scale bar, 50 nm.)

anhydrous methods, which avoid aqueous solution-induced mineral phase transformations, obfuscate intracellular processes and disrupt organic cellular components (19). Therefore, to better understand our observations of intracellular calcium phosphate, we prepared mineralized nodules using a combination of high-pressure freezing (HPF) and freeze substitution (FS). These methods prompt the formation of amorphous ice that is subsequently replaced by organic solvents at low temperatures (20), ensuring close-to-native preservation of cellular structures, mineral composition, morphology, and exceptionally, the distribution of ions (21). We then used high angle-annular dark-field scanning TEM (HAADF-STEM) and electron energy-loss spectroscopy (EELS)—a technique that allows determination of the elemental composition of the sample—to examine the mineralization process.

When we examined osteoblast and MSC nodules prepared by HPF-FS, not only was calcium phosphate evident within intracellular vesicles, but bright-field TEM and HAADF-STEM imaging also confirmed its presence within mitochondria (Fig. 2 *A* and *B*, respectively, and Fig. S5). EELS analysis of mitochondrial granules, which were tens of nanometres in diameter (47.6 ± 16.8 nm, $n = 50$), identified characteristic phosphorus $L_{2,3}$ and calcium $L_{2,3}$ edges at 132 and 346 eV, respectively (Fig. 2*C*), with phosphorus $L_{2,3}$ edge characteristics indicative of phosphate compounds (22). Areas within the mitochondrial matrix that were devoid of such electron-dense granules, however, also sometimes produced the characteristic calcium edge (Fig. 2*C*, MM2). This observation, which was only possible because HPF-FS allows for preservation of ions, is consistent with previous reports that mitochondria maintain considerable stores of ionic calcium in addition to granules (23). Further analysis of the mitochondrial granules with bright-field TEM (Fig. 2*D*) revealed globular accumulations with disordered morphologies.

Mitochondrial granules have been previously described (24, 25), and indirect evidence, including reports of granule depletion in cells at the mineralization front (10, 26), has led many investigators to speculate a role for mitochondrial granules in bone mineralization (10, 23, 27, 28), perhaps by storing calcium and phosphate ions and later making them available for bone mineralization. Others have similarly speculated a relationship between mitochondrial granules and mineral-containing vesicles, because granule depletion in epiphyseal chondrocytes manifests concurrently with the appearance of extracellular mineral-containing vesicles (28). Nevertheless, direct observations linking intramitochondrial calcium and phosphate deposits with vesicles and the extracellular mineralization process, have thus far been lacking. Our analyses of both osteoblast and MSC nodules with HAADF-STEM, however, revealed vesicles intimately associated with granule-containing mitochondria (Fig. 3*A* and Fig. S6). Reconstructed 3D tomograms of HAADF-STEM images captured at incremental tilt angles showed mitochondria and vesicles as distinct entities, but with notable membrane discontinuities at their conjoining interfaces (Fig. 3*B* and Movie S1). Chemical analysis of the dense mitochondrial granules and the interior of associating vesicles by EELS further indicated the presence of calcium (Fig. 3*C* and Figs. S7 and S8). Moreover, images collected from orthoslices through the vesicle-mitochondrial interface revealed discontinuities in the mitochondrial membrane, suggesting their fusion (Fig. 3*D*).

Our observations of intracellular calcium-containing vesicles and their role in extracellular mineralization provide support for hypotheses suggesting that intracellular processes contribute to bone apatite formation. Anderson has long implicated mineral-containing vesicles in biological mineralization (29). Proteins and enzymes associated with vesicular membranes, combined with their specific lipid composition, are thought to provide a protective nidus for the precipitation of calcium phosphate. However, although Anderson described vesicles accumulating mineral extracellularly, our observations here highlighting a step-by-step process by which intravesicular amorphous calcium phosphate is transported from the intra- to extracellular space provides a direct link between Mahamid et al.'s (12) observations of intracellular vesicles and extracellular vesicles that associate with the ECM (29).

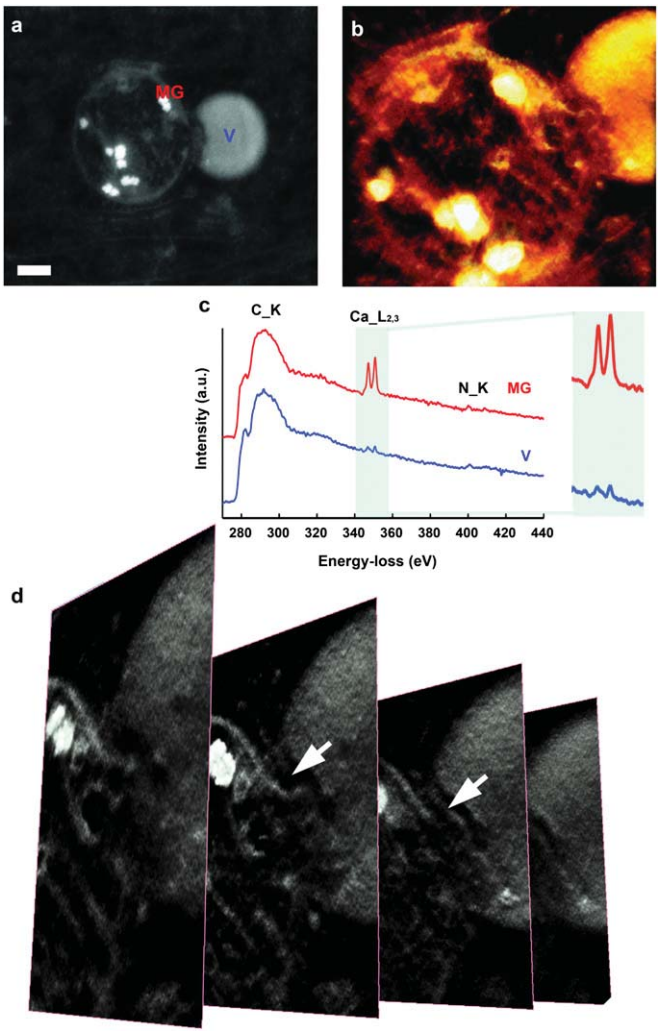

Fig. 3. Analytical electron microscopy evidence of vesicle-mitochondrial interactions in mineralizing osteoblasts. (*A*) HAADF scanning TEM image of a dense granule-containing mitochondrion associating with a vesicle within an osteoblast in a mineralized nodule. The sample was prepared by HPF-FS. (Scale bar, 200 nm.) (*B*) Voltex projection of a 3D tomography reconstruction showing a mitochondrion conjoined with a vesicle. Dense granules are evident within the mitochondrion. See Movie S1 for the full reconstruction demonstrating a discontinuity in the mitochondrial membrane where it conjoins the vesicle. Sample was prepared by HPF-FS. (*C*) EELS of specified areas within the mitochondrion and vesicle in *A*. The mitochondrial granule and vesicle show characteristic calcium $L_{2,3}$ edges at 346 eV. All spectra display carbon K edges. (*D*) Orthoslices at 10-nm intervals through the tomography reconstruction showing the mitochondrion-vesicle interface. The mitochondrial membrane is discontinuous where it conjoins the vesicle (arrows).

Nucleation theory has been used to explain bone apatite formation because extracellular fluid is sufficiently saturated with respect to calcium and phosphate [perhaps stored as calcium-polyphosphate complexes (30)] to allow for mineral formation (31). However, recent insights into the role of amorphous mineral precursors in bone mineralization (3), and our and other's (12) observations of intracellular calcium and phosphorus-containing vesicles, suggests that active transport of mineral from the intra- to the extracellular space may play a role in bone apatite

formation. Our observations of calcium and dense calcium- and phosphate-containing granules within mitochondria, together with published accounts of temporal relationships between mitochondrial granule depletion and the onset of extracellular mineralization (10), strongly point toward an association between mitochondria, intracellular calcium phosphate accumulations, and the mineralization process. Our observation that calcium phosphate or calcium exists both within mitochondria and intracellular vesicles suggests that a mechanism may exist in osteogenic cells by which ionic calcium (and perhaps phosphate) are transferred from mitochondria to intracellular vesicles, possibly via a simple process, such as diffusion. Supporting other studies (23), these data further suggest that mitochondrial granules may act as a storage depot for calcium and phosphate, allowing perhaps for subsequent dissolution and transport of ions required for bone formation. Although the unregulated disruption of the mitochondrial membrane is ordinarily implicated in cell death and apoptosis, there is increasing evidence that regulated vesicular transport may occur between mitochondria and other cellular organelles. For example, iron may be transported to the mitochondria via endosomes (32), and more recent studies have shown that membranous vesicles bud off from mitochondria, transporting fatty acids to the peroxisome (33). The data presented here suggest a role for mitochondria in the trafficking of ions or clusters of calcium and phosphate ions to the extracellular space, facilitating mammalian mineralization.

Although some authors have questioned the presence of an amorphous phase in bone mineral, strong evidence for amorphous calcium phosphate within mitochondrial granules (24) and newly formed bone (3, 5) exists. Furthermore, recent in vitro studies have elucidated mechanisms by which transiently formed clusters of calcium and phosphate ions could become orientated bone apatite via a synergistic interplay between collagen structure and nucleation inhibitors (6, 7). Mitochondrial globular mineral deposits examined here were ~50 nm in diameter and were composed of smaller globules with disordered morphologies. This finding is consistent with Dey et al.'s report in which amorphous mineral globules created in a surface-induced nucleation model were only stable up to diameters of ~50 nm (7). The finding also supports Mahamid et al.'s observations that vesicle-enclosed, intracellular calcium phosphate is composed of 80-nm globules, which in turn are composed of smaller 10-nm globules (12). Moreover, such disordered globules are similar to those detected in the mineralizing fin ray bones of zebrafish (3), suggesting a link between the intracellular calcium phosphate detected in our in vitro model and that identified in mineralizing native bone.

Despite this finding, few studies have yet attempted to address how intracellular calcium phosphate might be translated to mature

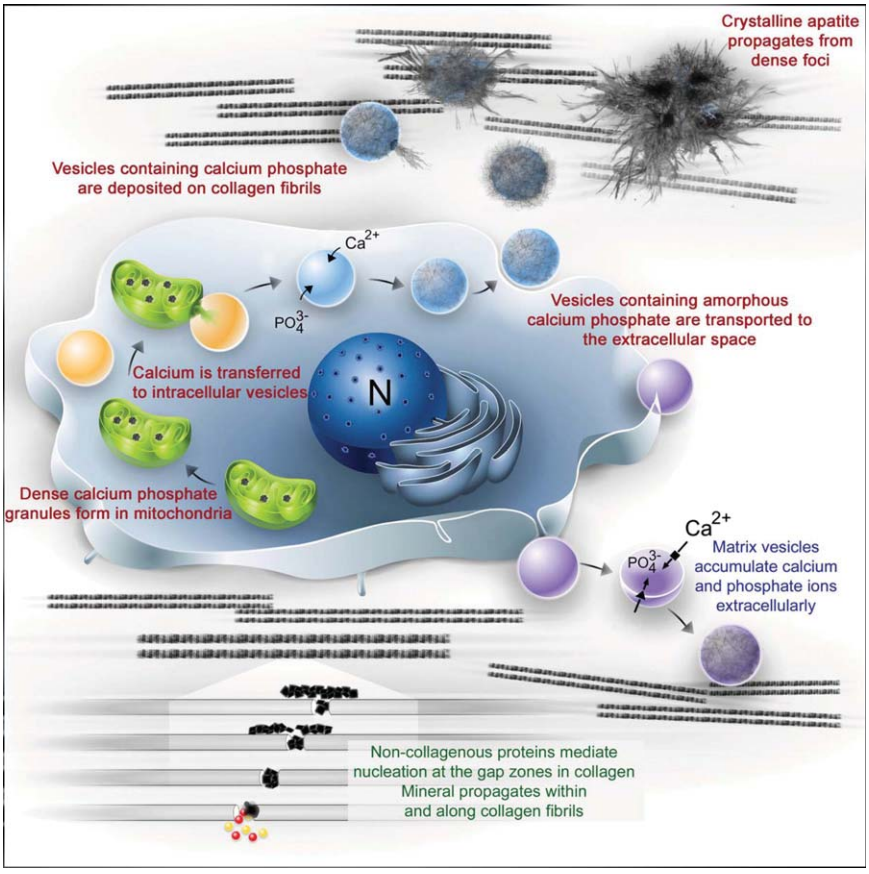

Fig. 4. Diagram outlining current models and our proposed mechanism for bone mineral formation. Bone apatite formation likely proceeds via a number of cooperative/redundant mechanisms. Current hypotheses include the utilization of: (*i*) Matrix vesicles which bud from the plasma membrane and accumulate calcium (Ca^{2+}) and phosphate (PO_4^{3-}) ions extracellularly before associating with the collagenous ECM (2); (*ii*) Noncollagenous proteins associated with the gap zones in collagen, which mediate mineral nucleation and foster its propagation within and along collagen fibrils (1); and (*iii*) Our suggested model, by which amorphous calcium phosphate and ionic calcium stored in mitochondria is transported via vesicles to the ECM before converting to more crystalline apatite and propagating from dense foci. In the cartoon, "matrix vesicles" are purple, and collagen-mediated mineralization is depicted in the bottom left corner with calcium and phosphate ions highlighted in yellow and red. Mitochondria are shown in green, and vesicles are orange and blue, with and without mineral/ions, respectively. "N" identifies the cell nucleus.

ECM-associated bone apatite. Lehninger postulated that calcium phosphate packets might be extruded from mitochondria and make their way to the ECM to participate in bone formation (34). Shapiro and Greenspan likewise speculated that mitochondrial granules may be released into the cytoplasm as calcium and phosphate ions, and eventually contribute to extracellular mineral formation (27), and Sayegh et al. suggested mitochondria might move to a peripheral position in the cytoplasm before releasing their contents (10). Our observations here, that direct transport of ions of calcium and possibly phosphate takes place between mitochondria and intracellular vesicles, provides a missing link in deciphering the process of normal bone mineral formation.

Fig. 4 details a proposed model for bone mineral formation involving mitochondrial granules, calcium- and phosphorus-containing vesicles, and extracellular mineral precipitation. The diagram also takes into account previous observations of extracellular vesicles accumulating mineral, collagen-based mineralization, and our observations of intracellular calcium phosphate and its transport to the ECM. Indeed, as others have noted (4), all of these processes may occur concurrently, as a certain degree of redundancy is likely inherent in biomineralization. Nonetheless, this model provides fresh insight into our fundamental understanding of bone mineralization, and may have important implications for understanding and treating pathological mineralization.

Materials and Methods

Cell Culture. Mineralized nodules were formed from cells derived from neonatal mouse calvarial osteoblasts and adult mouse MSC, as previously described (14). For a thorough description of methods, see *SI Materials and Methods*. Briefly, for osteoblast cultures, calvaria were removed from 2-d-old pups, mechanically minced, enzymatically digested, and cultured. For MSC cultures, marrow was flushed from mouse tibiae and femora and adherent cells were cultured. To initiate mineralized nodule formation, 30,000 cells/cm^2 were plated on sapphire discs or glass cover-slips and cultured for 28 d in medium containing ascorbic acid and β-glycerophosphate.

Sample Preparation. Fixation of mineralized nodules for electron microscopy can affect both the organic and inorganic components of the sample. Please see *SI Materials and Methods* for a detailed description of sample preparation considerations.

Chemical fixation. Mineralized cultures were fixed in glutaraldehyde, post-fixed in osmium tetroxide, dehydrated in a graded ethanol series, treated with acetronitrile, and finally infiltrated with a Quetol-based resin, as previously described (14). For a full description, see *SI Materials and Methods*. Embedded samples were polymerized at 60 °C for 24 h, sectioned (70 nm) into a water bath using a diamond knife, and collected on bare 300 mesh copper TEM grids.

Anhydrous fixation. Cultures were dehydrated in ethylene glycol (24) for 3 h, immersed in fresh acetronitrile three times for 10 min each, infiltrated, cured in resin, and sectioned onto TEM grids.

HPF-FS. Samples were cryofixed in a HPF apparatus and freeze-substituted in an anhydrous acetone solution containing glutaraldehyde, osmium, and uranyl acetate. Samples were infiltrated with resin as described above.

Electron Microscopy Studies. All TEM observations were made after viewing several hundred cells from multiple areas of at least three separate cell cultures. Bright-field TEM, SAED, and EDX were performed on a JEOL 2000FX, operated at 120 kV. Bright-field TEM, HAADF-STEM, and STEM- EELS were performed on a Titan 80/300 STEM/TEM operated at 300 kV using a 4 kV extraction voltage. For 3D-tomography, images were acquired in HAADF-STEM mode at 2° increments from −45° to +45°. Three-dimensional reconstruction was carried out using the simultaneous iterative reconstruction algorithm using Inspect 3D image processing software (FEI). Reconstructions were visualized and isosurface projections and orthoslices were created using Amira 3D visualization software (Mercury Computer Systems). For a full description of electron microscopy studies, see *SI Materials and Methods*.

ACKNOWLEDGMENTS. This work was supported in part by a fellowship from the Royal Thai Government (to S.B.); a career development fellowship from the Medical Research Council (to N.D.E.); the European Union Seventh Framework Programme, Project 257182 (Carbon Nanotubes at the Blood Brain Barrier) (to A.E.P.); and a European Research Council Starting Investigator grant (Naturale) (to M.M.S.).

1. Glimcher MJ (1984) Recent studies of the mineral phase in bone and its possible linkage to the organic matrix by protein-bound phosphate bonds. *Philos Trans R Soc Lond B Biol Sci* 304:479–508.
2. Anderson HC (1995) Molecular biology of matrix vesicles. *Clin Orthop Relat Res* (314): 266–280.
3. Mahamid J, Sharir A, Addadi L, Weiner S (2008) Amorphous calcium phosphate is a major component of the forming fin bones of zebrafish: Indications for an amorphous precursor phase. *Proc Natl Acad Sci USA* 105:12748–12753.
4. Boskey AL (1998) Biomineralization: Conflicts, challenges, and opportunities. *J Cell Biochem Suppl* 30–31:83–91.
5. Mahamid J, et al. (2010) Mapping amorphous calcium phosphate transformation into crystalline mineral from the cell to the bone in zebrafish fin rays. *Proc Natl Acad Sci USA* 107:6316–6321.
6. Nudelman F, et al. (2010) The role of collagen in bone apatite formation in the presence of hydroxyapatite nucleation inhibitors. *Nat Mater* 9:1004–1009.
7. Dey A, et al. (2010) The role of prenucleation clusters in surface-induced calcium phosphate crystallization. *Nat Mater* 9:1010–1014.
8. Weiner S (2008) Biomineralization: A structural perspective. *J Struct Biol* 163:229–234.
9. Martin JH, Matthews JL (1970) Mitochondrial granules in chondrocytes, osteoblasts and osteocytes. An ultrastructural and microincineration study. *Clin Orthop Relat Res* 68:273–278.
10. Sayegh FS, Solomon GC, Davis RW (1974) Ultrastructure of intracellular mineralization in the deer's antler. *Clin Orthop Relat Res* (99):267–284.
11. Sutfin LV, Holtrop ME, Ogilvie RE (1971) Microanalysis of individual mitochondrial granules with diameters less than 1000 angstroms. *Science* 174:947–949.
12. Mahamid J, et al. (2011) Bone mineralization proceeds through intracellular calcium phosphate loaded vesicles: A cryo-electron microscopy study. *J Struct Biol* 174: 527–535.
13. Malaval L, Liu F, Roche P, Aubin JE (1999) Kinetics of osteoprogenitor proliferation and osteoblast differentiation in vitro. *J Cell Biochem* 74:616–627.
14. Gentleman E, et al. (2009) Comparative materials differences revealed in engineered bone as a function of cell-specific differentiation. *Nat Mater* 8:763–770.
15. Boskey AL, Posner AS (1973) Conversion of amorphous calcium phosphate to microcrystalline hydroxyapatite–Ph-dependent, solution-mediated, solid-solid conversion. *J Phys Chem-Us* 77:2313–2317.
16. Hoshi K, Ozawa H (2000) Matrix vesicle calcification in bones of adult rats. *Calcif Tissue Int* 66:430–434.
17. Anderson HC (1967) Electron microscopic studies of induced cartilage development and calcification. *J Cell Biol* 35:81–101.
18. Arana-Chavez VE, Massa LF (2004) Odontoblasts: The cells forming and maintaining dentine. *Int J Biochem Cell Biol* 36:1367–1373.
19. Landis WJ, Paine MC, Glimcher MJ (1977) Electron microscopic observations of bone tissue prepared anhydrously in organic solvents. *J Ultrastruct Res* 59:1–30.
20. McDonald KL, Auer M (2006) High-pressure freezing, cellular tomography, and structural cell biology. *Biotechniques* 41:137–143.
21. Budka D, Mesjasz-Przybylowicz J, Tylko G, Przybylowlicz WJ (2005) Freeze-substitution methods for Ni localization and quantitative analysis in Berkheya coddii leaves by means of PIXE. *Nucl Instrum Methods Phys Res B* 231:338–344.
22. Kruse J, et al. (2009) Phosphorus L(2,3)-edge XANES: Overview of reference compounds. *J Synchrotron Radiat* 16:247–259.
23. Lehninger A (1970) Mitochondria and calcium ion transport—Fifth Jubilee Lecture. *Biochem J* 119:128–138.
24. Landis WJ, Glimcher MJ (1978) Electron diffraction and electron probe microanalysis of the mineral phase of bone tissue prepared by anhydrous techniques. *J Ultrastruct Res* 63:188–223.
25. Landis WJ, Hauschka BT, Rogerson CA, Glimcher MJ (1977) Electron microscopic observations of bone tissue prepared by ultracryomicrotomy. *J Ultrastruct Res* 59: 185–206.
26. Martin JH, Matthews JL (1969) Mitochondrial granules in chondrocytes. *Calcif Tissue Res* 3:184–193.
27. Shapiro IM, Greenspan JS (1969) Are mitochondria directly involved in biological mineralisation? *Calcif Tissue Res* 3:100–102.
28. Brighton CT, Hunt RM (1976) Histochemical localization of calcium in growth plate mitochondria and matrix vesicles. *Fed Proc* 35:143–147.
29. Anderson HC (2003) Matrix vesicles and calcification. *Curr Rheumatol Rep* 5:222–226.
30. Omelon S, et al. (2009) Control of vertebrate skeletal mineralization by polyphosphates. *PLoS ONE* 4:e5634.
31. Posner AS, Betts F, Blumenthal NC (1978) Properties of nucleating systems. *Metab Bone Dis Relat Res* 1:179–183.
32. Sheftel AD, Zhang AS, Brown C, Shirihai OS, Ponka P (2007) Direct interorganellar transfer of iron from endosome to mitochondrion. *Blood* 110:125–132.
33. Neuspiel M, et al. (2008) Cargo-selected transport from the mitochondria to peroxisomes is mediated by vesicular carriers. *Curr Biol* 18:102–108.
34. Lehninger A (1977) Mitochondria and biological mineralization processes: An exploration. *Horizons in Biochemistry and Biophysics*, eds Qualiariello E, Palmieri F, Singer T (Addison Wesley, Reading, MA), Vol 4.

Supporting Information

Boonrungsiman et al. 10.1073/pnas.1208916109

SI Materials and Methods

Cell Culture. Neonatal mouse calvarial osteoblasts and adult mouse marrow stromal cells were cultured to form mineralized nodules as previously described by Gentleman et al. (1).

Neonatal mouse calvarial osteoblasts. Osteoblasts were derived from 2-d-old neonatal CD-1 mice. Mice were killed by cervical dislocation according to Imperial College London ethical guidelines and calvarial tissue from all of the pups in a litter were removed and pooled. Calvaria were washed in PBS and soft tissue was carefully removed before calvaria were minced with scissors. Minced calvaria were subjected to five digests at 37 °C in a 1-mg/mL solution of collagenase (Sigma) in Hank's Balanced Salt Solution supplemented with a 10% (vol/vol) solution of 0.05% (wt/vol) trypsin/EDTA (both from Invitrogen). The first four digests were carried out for 20 min each, followed by a fifth digest for 2 h. Supernatants from the last three digests were centrifuged to collect cells and plated in α-minimum essential medium (αMEM) supplemented with 15% (vol/vol) FBS and a 1× solution of penicillin/streptomycin (P/S) (all from Invitrogen). Cells from the third or fourth passage were used in experiments.

Mouse marrow stromal cells. Mouse marrow stromal cells (MSC) were isolated from the marrow stroma of femora and tibiae from 6-wk-old FVB/N female mice. After the mice were killed by cervical dislocation, femora and tibiae were removed and carefully cleaned of soft tissue. The bone epiphyses were then removed with scissors and diaphyses were repeatedly flushed with αMEM supplemented with 15% (vol/vol) FBS and 1× P/S. Extracted marrow from all animals was pooled and plated on standard tissue-culture plastic. Culture media was changed on days 4 and 8 after harvest and cells were passaged starting on day 9. Only cells up to the third passage were used in experiments.

Mineralized nodule formation. To induce mineralized nodule formation, cells were plated on sapphire discs (Leica Microsystems) or glass cover-slips (for sample preparation by high pressure freezing and chemical/anhydrous fixation, respectively) at 30,000 cells/cm^2 in αMEM supplemented with 15% (vol/vol) FBS, 1× P/S, 50 μg/mL ascorbic acid, and 10 mM β-glycerophosphate (both from Sigma), according to a widely used protocol for in vitro differentiation of mineralizing cells (2). Dexamethasone was added to all cultures at a concentration of 1 μM beginning at day 14 and cultivation was continued until day 28. Culture medium was changed every 2 d.

Sample Preparation. Nodules formed from mineralizing cell cultures contain both organic and mineral components (1). To effectively and accurately analyze both the cells and the material they form, it is essential to minimize alterations to cell ultrastructure, while also preserving the distribution, crystallinity, and chemistry of the mineral during preparation and analysis by transmission electron microscopy (TEM). The artifacts that can be introduced during sample preparation for TEM can be subtle; therefore, the use of several complementary techniques in parallel should allow for accurate analysis. In this study, we used three techniques: an anhydrous preparation protocol, room temperature chemical fixation, and high-pressure freezing combined with freeze substitution (HPF-FS). Chemical fixation is a preparation protocol routinely used to prepare animal cells for TEM studies. This method chemically cross-links the proteins within the tissue; however, the chemical fixation changes mineral crystallinity (3) because the aqueous solution causes the conversion of noncrystalline calcium phosphate to thermodynamically stable crystalline hydroxyapatite (4, 5). An alternative room-temperature preparation technique is to use a completely anhydrous method, which preserves the crystallinity of the apatite (3, 6, 7); however, this method does not chemically cross-link the proteins, so the ultrastructure of the organic components (in this case, cell organelles) are poorly preserved. HPF-FS simultaneously chemically cross links proteins while also preserving ion distributions within the sample. This method only introduces 1% water into the sample; therefore, the amount of amorphous calcium phosphate that is converted to crystalline hydroxyapatite should be very low. This method reportedly maintains the stability of disordered calcium phosphate (4) and can be used to study the morphology of calcium phosphate; however, the fully anhydrous method remains the most suitable for diffraction analyses. Mineralized nodules are ~100–200 μm thick (1); for this reason HPF followed by FS with acetone was selected as a suitable method to prepare samples for electron energy-loss spectroscopy (EELS) analysis. The HPF-FS protocol was optimized for the mineralized nodules studied here. The ultrastructure, morphology, and chemistry of the mineral in the samples prepared by HPF-FS was compared with that within nodules prepared by conventional chemical fixation and anhydrous methods. The HPF-FS method preserved both the ultrastructure and mineral morphology, and also preserved the chemistry and the distribution of calcium ions within the nodules.

Chemical fixation. Samples were fixed in 4% (vol/vol) glutaraldehyde in 0.1 M PIPES buffer at 4 °C for 2 h, and then postfixed in 1% (wt/vol) osmium tetroxide in 0.1 M PIPES buffer for 1 h at room temperature (all from Sigma). Samples were then dehydrated in a graded ethanol series of three successive baths of 50%, 70%, 90%, and 100% (vol/vol) ethanol for 5 min each and submerged three times in acetronitrile (Sigma) for an additional 10 min each, all at room temperature. After dehydration, samples were progressively infiltrated with a Quetol-based resin, created by combining 12.6 g quetol, 15.5 g nonenyl succinic anhydride, 6.5 g methyl nadic anhydride, and 0.6 g benzyl dimethylamine (all from Agar Scientific). This solution was mixed with acetonitrile at a ratio of 1:1 (resin:acetonitrile) and samples were infiltrated for 2 h followed by infiltration in a 3:1 ratio solution overnight, and finally in pure resin for 4 d with fresh resin replaced daily. Embedded samples were then polymerized at 60 °C for 24 h. Thin sections (70 nm) were cut directly into a water bath using an ultramicrotome with a diamond knife set at an angle of 35°. Sections were immediately collected on bare, 300 mesh copper TEM grids (Agar Scientific) and dried on filter paper.

Anhydrous method. Cultures were dehydrated in ethylene glycol (Sigma) for 3 h, as previously described (3), and then immersed in fresh acetronitrile three times for 10 min each. Samples were infiltrated, cured in a Quetol-based resin, and thin sectioned onto TEM grids using the methods described above.

HPF-FS. Samples were placed in specimen carriers with 200-μm deep cavities, mounted in a 20% (wt/vol) solution of bovine serum albumin (Sigma) in αMEM, and frozen using a Leica EM PACT 2 (Leica Microsystems) high-pressure freezer. Freeze substitution was performed in a Leica electron microscope AFS2 freeze substitution device using an anhydrous solution of acetone containing a 3% (vol/vol) glutaldehyde, 1% (wt/vol) osmium tetroxide, and 0.5% (wt/vol) uranyl acetate at −90 °C for 8 h. Samples were then gradually warmed to 0 °C at 5 °C/h, washed

twice in acetone, brought to room temperature, and infiltrated with resin, as described above.

Analytical Electron Microscopy Studies. All electron microscopy observations were made after viewing several hundred cells from multiple sample areas from at least three independent cell cultures for each cell type. The electron dose was kept to a minimum to minimize radiation damage to the mineral phase.

Electron microscopy. Bright-field TEM, selected area electron diffraction (SAED) and energy dispersive X-ray spectroscopy (EDX) were performed on a JEOL 2000FX, operated at 120 kV. Bright-field TEM, high angle-annular dark field scanning transmission electron microscopy (HAADF-STEM), and STEM-EELS were performed on a Titan 80/300 STEM/TEM operated at 300 kV using a 4 kV extraction voltage. EELS was carried out in STEM mode under the same operating conditions. The convergence and collection semiangle into the spectrometer were set to 6.80 and 8.90 mrad, respectively. The energy resolution was 0.9 eV and the dispersion was set to 0.1 and 0.2 eV per pixel to collect one characteristic edge per spectrum, and all characteristic edges of phosphorus and calcium in a single spectrum, respectively. EELS spectra were acquired from an area that had a relative thickness (t/λ) of less than 0.5. Spectra were background subtracted using a power law model, smoothed with a Savitzky-Golay filter (8), intensity normalized to the carbon K edge, and shifted along the *y* axis.

Three-dimensional tomography. Three-dimensional tomography images were acquired at 300 kV in HAADF-STEM mode. Images were acquired at 2° increments from −45° to +45° using HAADF detector with inner and outer collection semiangle of 40 and 196 mrad, respectively. Three-dimensional reconstructions were carried out using the simultaneous iterative reconstruction technique (9) using Inspect 3D image processing software (FEI). Reconstructions were visualized by a Voltex projection and orthoslices through the HAADF-STEM reconstructions using Amira 3D visualization software (Mercury Compter Systems). Visualizations of 3D reconstructions were also carried out by creating isosurfaces based on the levels of intensity of regions within the tomographic dataset. An opaque isosurface was created at a higher intensity level to represent only those regions within the cell volume, which were of particularly high intensity corresponding to the calcium phosphate granules.

1. Gentleman E, et al. (2009) Comparative materials differences revealed in engineered bone as a function of cell-specific differentiation. *Nat Mater* 8: 763–770.
2. Malaval L, Liu F, Roche P, Aubin JE (1999) Kinetics of osteoprogenitor proliferation and osteoblast differentiation in vitro. *J Cell Biochem* 74:616–627.
3. Landis WJ, Glimcher MJ (1978) Electron diffraction and electron probe microanalysis of the mineral phase of bone tissue prepared by anhydrous techniques. *J Ultrastruct Res* 63:188–223.
4. Boskey AL, Posner AS (1973) Conversion of amorphous calcium phosphate to microcrystalline hydroxyapatite. A pH-dependent, solution-mediated, solid-solid conversion. *J Phys Chem* 77:2313.
5. Combes C, Rey C (2010) Amorphous calcium phosphates: Synthesis, properties and uses in biomaterials. *Acta Biomater* 6:3362–3378.
6. Porter AE, Patel N, Skepper JN, Best SM, Bonfield W (2004) Effect of sintered silicate-substituted hydroxyapatite on remodelling processes at the bone-implant interface. *Biomaterials* 25:3303–3314.
7. Thurner PJ, et al. (2010) Osteopontin deficiency increases bone fragility but preserves bone mass. *Bone* 46:1564–1573.
8. Savitzky A, Golay MJE (1964) Smoothing and differentiation of data by simplified least squares procedures. *Anal Chem* 36:1627–1639.
9. Gilbert P (1972) Iterative methods for the three-dimensional reconstruction of an object from projections. *J Theor Biol* 36:105–117.

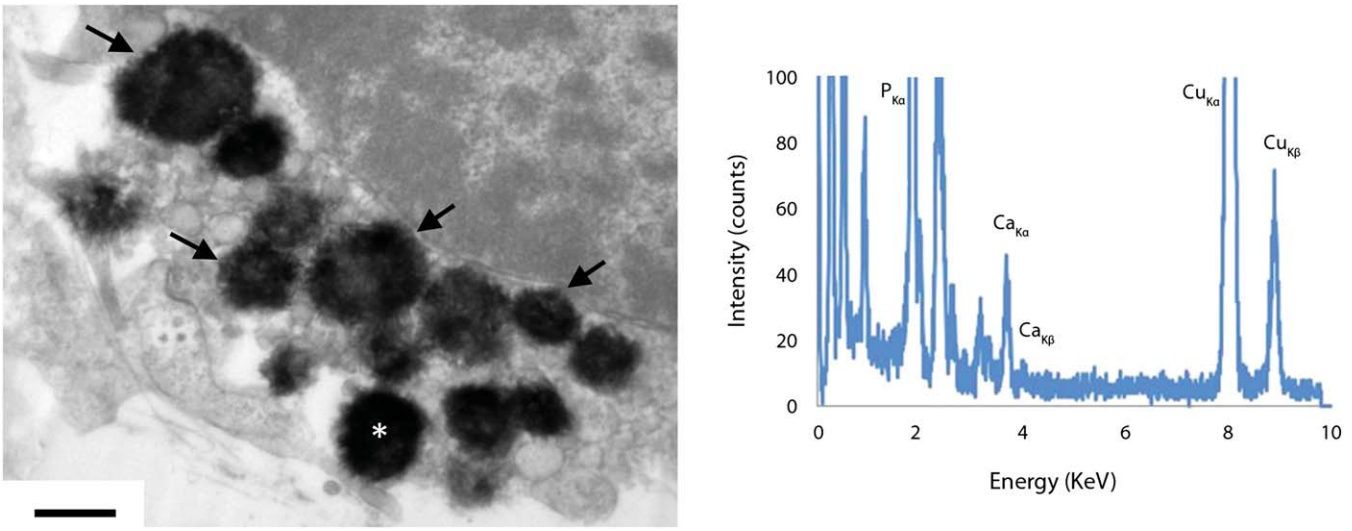

Fig. S1. Bright-field TEM micrograph highlighting vesicles enclosing electron-dense material (arrows) within an osteoblast. The osteoblast nodule was prepared by chemical fixation and poststained with uranyl acetate and lead citrate. (Scale bar, 500 nm.) An EDX spectrum taken from a vesicle (*) displays peaks for calcium and phosphorus.

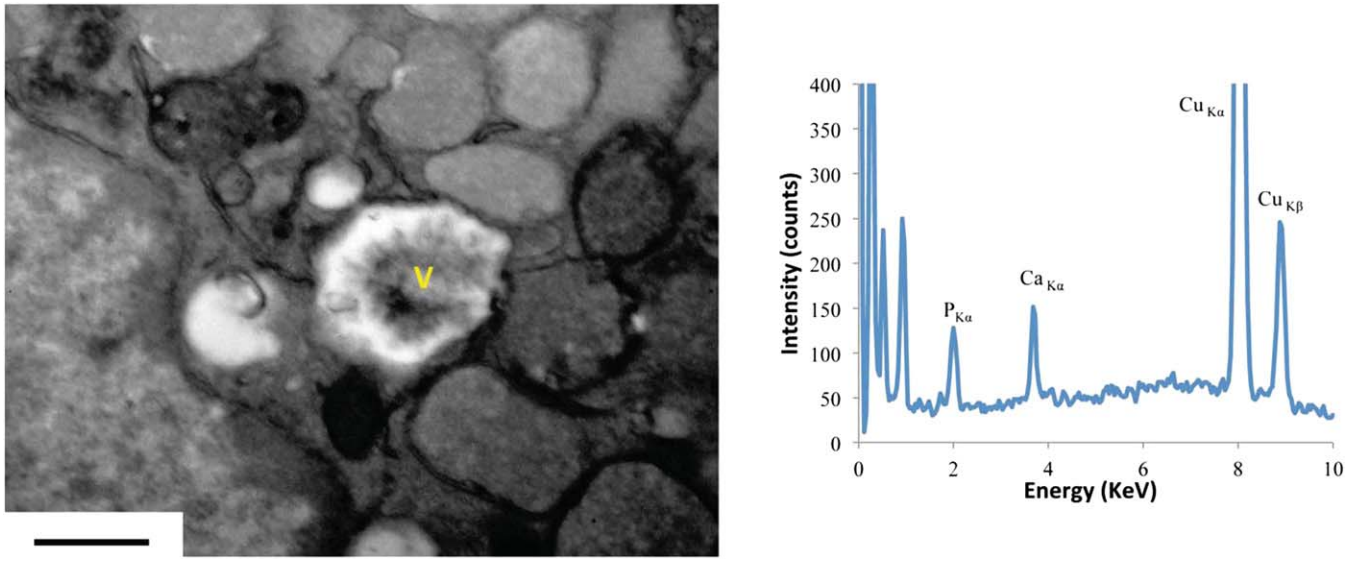

Fig. S2. Bright-field TEM micrograph of a vesicle (V) enclosing electron dense material within a mouse MSC. An EDX spectrum taken from the vesicle displays notable peaks for calcium and phosphorus. The MSC nodule was prepared by chemical fixation. (Scale bar, 500 nm.)

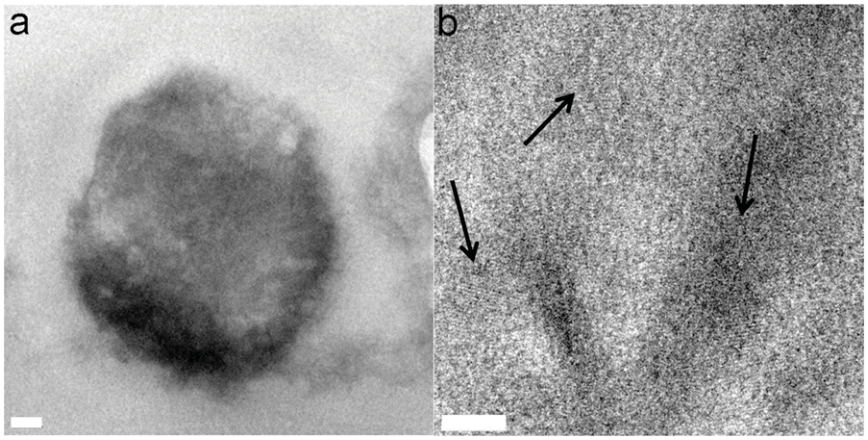

Fig. S3. (*A*) Bright-field TEM micrograph of a calcium phosphate-containing vesicle within a mineralized nodule prepared using the anhydrous method. (Scale bar, 50 nm.) (*B*) Phase-contrast image showing periodic lattice fringes (arrows) within the vesicle. (Scale bar, 5 nm.)

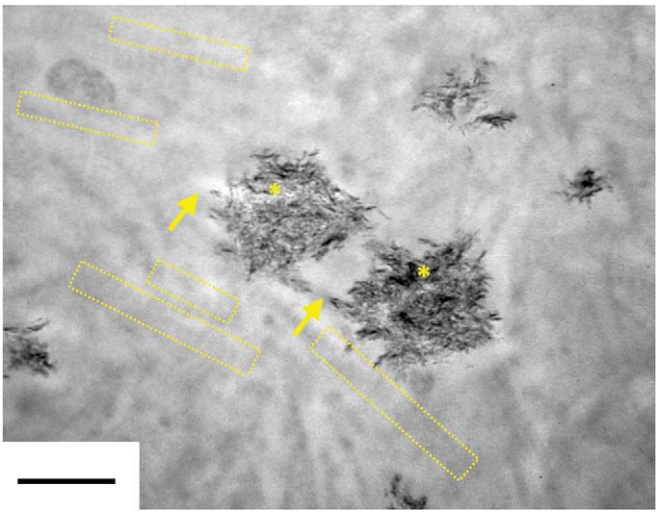

Fig. S4. Bright-field TEM micrograph of dense aggregates (*) associated with collagen fibrils (arrows) within the extracellular matrix of a nodule formed from MSC. Boxes indicate nonmineralized collagen fibrils. Samples were prepared by the anhydrous method. (Scale bar, 500 nm.)

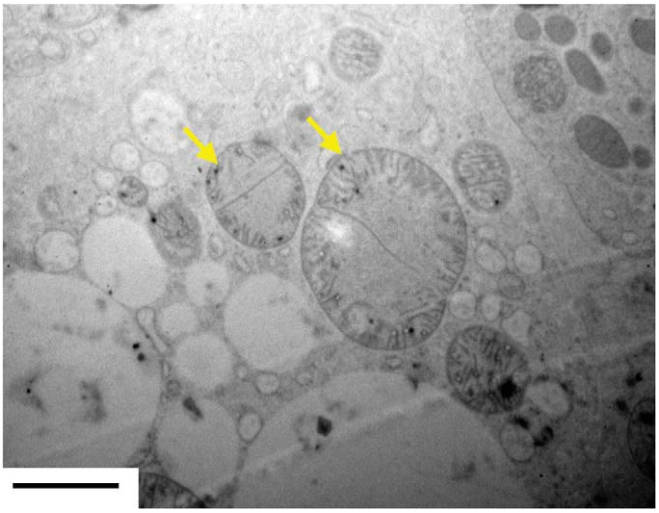

Fig. S5. Bright-field TEM image of dense granules inside mitochondria (arrows) within a MSC. Nodules were prepared by HPF-FS. (Scale bar, 1 μm.)

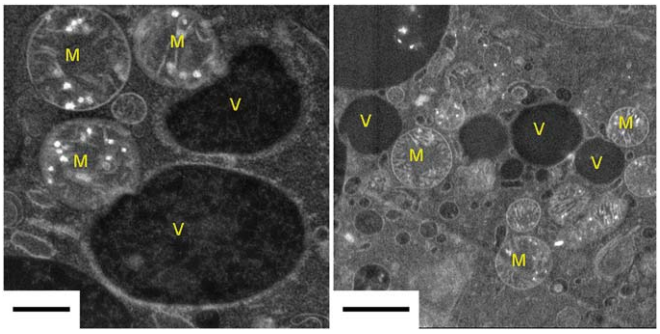

Fig. S6. HAADF-STEM images showing vesicles (V) in MSC, which were frequently observed closely associating with mitochondria (M). Samples were prepared by HPF-FS. [Scale bars, 1 μm (*Right*) and 500 nm (*Left*).]

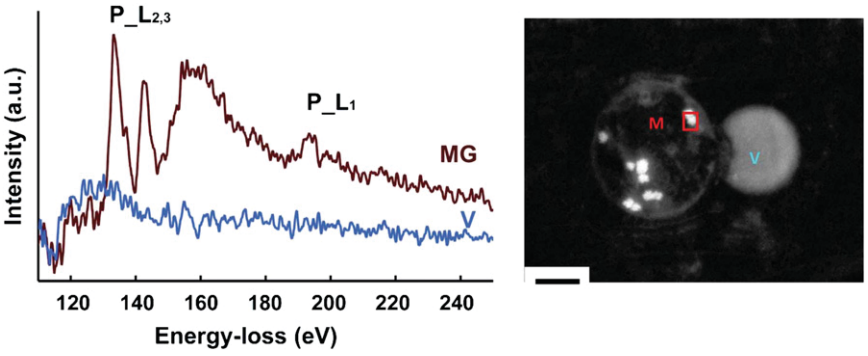

Fig. S7. Electron energy loss spectrum near the phosphorus edge for specified areas within a mitochondrion and an associated vesicle within a mineralizing osteoblast. Image (*Right*) is reproduced from Fig. 3*A* (Scale bar, 200 nm) and was prepared by HPF-SF. "MG" and "V" indicate the positions at which spectra were collected and highlight the presence phosphorus in the dense granule (MG); a distinct phosphorus edge was not detectable within the interacting vesicle (V). The lack of phosphorus detection by EELS does not rule of the possibility of the presence of phosphorus inside this vesicle. The calcium $L_{2,3}$ edge is narrow and sharp, but the phosphorus $L_{2,3}$ is relatively more broad and less intense. This finding suggests that the intensity of the phosphorus $L_{2,3}$ edge is below the signal-to-noise ratio of the instrument. Therefore, given the low intensity of the calcium edge (Fig. 3*C*), it is improbable that a phosphorus edge could be conclusively detected.

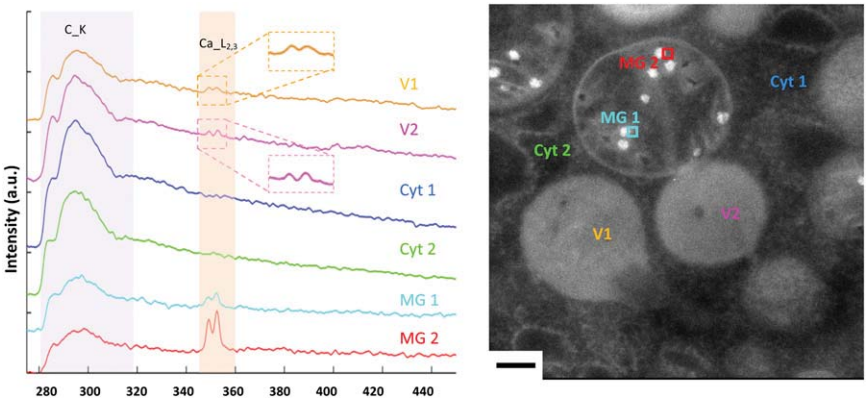

Fig. S8. EELS acquired from mitochondrial granules (MG), associating vesicles (V), and the surrounding cytoplasm (Cyt) in an osteoblast within a mineralizing nodule. The spectra of mitochondria granules display characteristic Ca $L_{2,3}$ edges at 346 eV. Spectra from the vesicles, one of which appears to be fused with the mitochondrion (V2) show a similar Ca $L_{2,3}$ edge. The surrounding cell cytoplasm did not produce characteristic Ca $L_{2,3}$ edges. Nodules were prepared by high pressure freezing and freeze substitution. (Scale bar, 200 nm.)

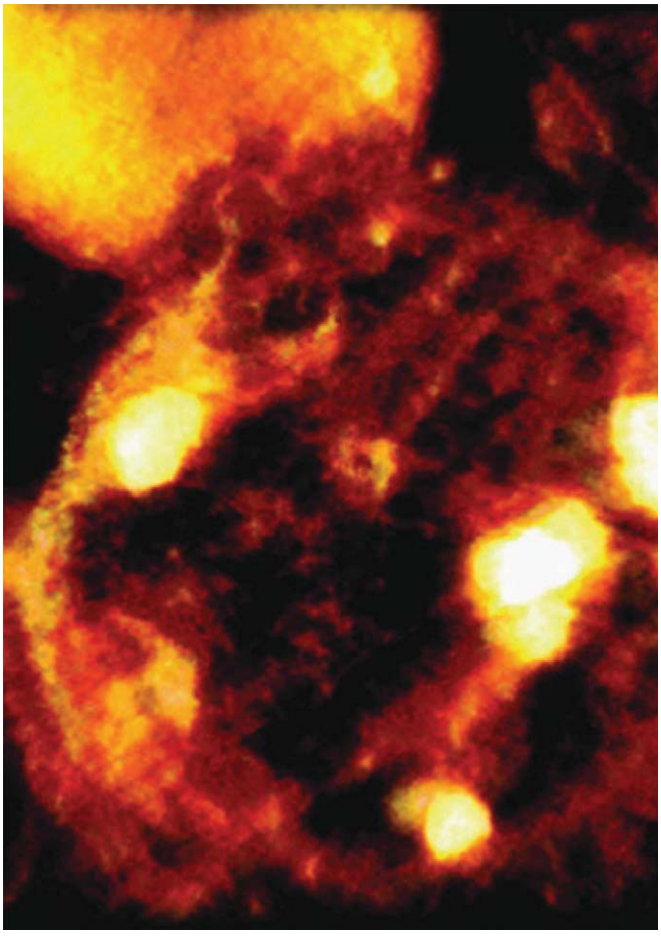

Movie S1. Movie of reconstructed tomograms captured by HAADF-STEM of oblique slices through the interface at which a mitochondrion and vesicle are joined. Dense granules appear bright in color and are apparent within the mitochondrion associated with its inner membrane. Movie was created from sample shown in Fig. 3*A*.

Movie S1